Arabian Journal for Science and Engineering (2023) 48:3783–3795
https://doi.org/10.1007/s13369-022-07254-x

RESEARCH ARTICLE-MECHANICAL ENGINEERING

Numerical Investigation of a Dual Fuel Engine Fueled by Diesel-Acetylene and Biodiesel-Acetylene with Modified Piston Bowl Geometry

G. Babusankar[1] · V. Manieniyan[1] · S. Sivaprakasam[1]

Received: 26 March 2022 / Accepted: 28 August 2022 / Published online: 15 September 2022

Abstract
Engine component design optimization plays an important role in enhancing the performance and emission characteristics of internal combustion engines. It has already been demonstrated that biodiesel-fueled compression ignition engines emit lower levels of emissions. The present work involves optimizing toroidal piston bowl geometry, in order to improve performance, emission, and combustion characteristics in dual fuel mode using diesel-acetylene and biodiesel-acetylene. The turbulence-creating tendency is utilized for optimizing piston bowl geometry to induce homogeneous mixture creation in the combustion chamber. To optimize the piston geometry physically is a time- and cost-consuming process, so the ANSYS-FLUENT CFD code is used to simulate the modified piston bowl geometries, where 1-, 1.5-, and 2-mm-diameter helical holes are placed in the surface of the crown to induce turbulence in the combustion chamber. Furthermore, 3, 4, and 5 holes are drilled in the crown surface for each diameter. The selection of optimum number of holes is carried out based on the analysis of turbulent intensity contours and the optimum hole diameter selection is based on the turbulent kinetic energy distribution. The results of the simulations show that the piston bowl of a diesel-acetylene fueled dual fuel engine with 5 holes of 1-mm-diameter piston geometry induces more turbulence than the other piston bowl geometries. Moreover, when compared to the other piston bowl geometries, the biodiesel-acetylene fueled dual fuel engine piston bowl with 5 holes of 2-mm-diameter piston geometry induces more turbulence.

Keywords Piston geometry · Dual fuel · Biodiesel · CFD · Helical hole

Abbreviations

aTDC	After top dead center
BTE	Brake thermal efficiency
bTDC	Before top dead center
CAD	Computer-aided design
CI	Compression ignition
CFD	Computational fluid dynamics
CO	Carbon monoxide
CNG	Compressed Natural Gas
EFI	End of the fuel injection
HC	Hydrocarbon
HCC	Hemispherical combustion chamber
IVC	Intake valve close
IC	Internal combustion
LPH	Liters per hour
LPG	Liquefied petroleum gas
LPM	Liters per minute
MAB	Microalgae biodiesel
NOx	Oxides of nitrogen
RNG	Re-Normalized Group
SCC	Shallow depth combustion chamber
SFI	Start of the fuel injection
SI	Spark ignition
TCC	Toroidal combustion chamber
TKE	Turbulent kinetic energy
TDC	Top dead center

✉ V. Manieniyan
manieniyan78@gmail.com

G. Babusankar
gbsr78@gmail.com

S. Sivaprakasam
rgssiva2002@gmail.com

[1] Department of Mechanical Engineering, Annamalai University, Chidambaram, India

List of Symbols

ρ	Density
c_{d}	Nozzle's discharge coefficient
$D_{\mathrm{d,stable}}$	Stable droplet diameter
D_{d}	Instantaneous droplet diameter
e	Specific internal energy
k	Turbulent kinetic energy
K_{c}	Form loss coefficient
K_{ε}	Empirical coefficient
L	Hole length
p	Pressure
q_{i}	Diffusive heat flux
Q_{H}	Heat source or sink per unit volume
S_{i}	Mass-distributed external force per unit mass
t_{b}	Characteristics time scale
U	Average injection velocity
u	Fluid velocity
ε	Turbulence dissipation rate
μ_{t}	Turbulent viscosity
μ	Dynamic viscosity
τ_{ij}	Viscous shear stress tensor
h	Thermal enthalpy

1 Introduction

Carbon emissions from the use of fossil fuels are causing serious environmental problems around the world. The majority of countries are on track to have zero carbon emissions by 2050. Because of the depletion of fossil fuels and growing environment concern, it is necessary to find alternate ways to mitigate the dependence on conventional fuels [36]. When compared to other energy conversion devices, compression ignition (CI) engines have the ability to convert and utilize a large amount of energy from oil [43]. However, the issue with CI engines is that they emit lot of greenhouse gases into the atmosphere [7]. Numerous studies are being conducted to decrease the emission levels, while improving performance. These studies include the use of alternative fuels, gaseous fuels, dual fuel technology, and engine component design modifications [42].

Biofuels are now a viable alternative to traditional diesel fuels [35]. Biofuels are primarily derived from non-edible plant sources like mahua, jatropha, karanja, sea mango, neem, linseed, and vegetable and animal wastes [44, 46]. Many countries have agreed to use a percentage of biofuels mixed with conventional diesel to reduce the reliance on fossil fuels [12]. The main advantage of blending a percentage of biofuel with diesel is that the efficiency and combustion properties are merely identical to pure diesel combustion whereas emitting less pollution [17, 34]. Many engine researchers discovered that the optimal biofuel-to-conventional diesel fuel blending ratio is around 20:80 [47]. [30] utilized blends of microalgae biodiesel in a single-cylinder CI engine with varying loads and compression ratios. The experimental results show that a 20% MAB blend significantly reduces NOx and smoke levels. [3] investigated the effects of modifying engine design parameters such as fuel injection pressure and nozzle geometry, fueled by Simarouba oil methyl ester (SuOME) in conventional diesel engine. The result shows that the modified engine parameters improves the performance and reduces the emission levels. [9] tested a single-cylinder CI engine fueled by egg shell catalyst and chicken waste biodiesel at variable engine speeds. The findings show that biodiesel blends improved BTE while lowering the emission levels. [48] examined the performance, emission, and combustion characteristics of a single-cylinder CI engine fueled by linseed biodiesel and discovered that the L30 blend fueled engine produced lower levels of CO and higher levels of NOx. [19] investigated the effect of B20 mahua biodiesel injected through a modified nozzle orifice diameter and discovered improved performance, emission, and combustion characteristics at partial loads when B20 mahua oil is injected through a smaller orifice diameter in comparison with diesel combustion. According to the literature, biodiesel can be used as an alternate to CI engines and is compatible with engine design modifications [33].

Gaseous fuels are gaining popularity among engine researchers due to their ability to burn completely with minimal carbon residue and to mix quickly with intake air [1]. Gaseous fuels such as LPG (liquefied petroleum gas) and CNG (compressed natural gas) are widely used as alternative gaseous fuels for CI engines and are unlikely to become obsolete in the near future. Although hydrogen gas has the potential to be utilized as an alternate gaseous fuel in CI engines, the process of storing and transporting is more complex and costly. As a result, it is stressful to discover an alternative gaseous fuel, such as acetylene, for use in CI engines. When gaseous fuel is supplied to the combustion chamber solely through the intake manifold, it has a lower volumetric efficiency because its density is lower than that of liquid fuels. [51] pioneered the use of acetylene gas in SI and CI engines in conjunction with alcohol. The result showed a considerable increase in BTE and reduced emission levels. Many researchers used acetylene in tandem with diesel in dual fuel operation [20]. [38] examined the SI engine fueled by various flow rates of acetylene in addition to gasoline fuel and discovered that the 100 LPH (Liters per hour) acetylene induction produces comparable performance and emissions characteristics to gasoline alone combustion. Some researchers used alternative liquid fuels and gaseous fuels in dual fuel operation [49]. [35] examined the acetylene-induced palm stearin biodiesel-fueled dual fuel engine and observed that 10 LPM acetylene gas injection improved biodiesel operation and obtained favorable emission charac-

teristics. By adding acetylene to the intake air, [25] improved the BTE and reduced emissions of a dual fuel engine fueled by Botryococcus braunii microalgae biodiesel.

Many researchers have proposed that engine parameters such as the intake manifold, combustion chamber geometry, injection pressure variation, and varying injection timing be optimized in order to achieve favorable fluid motion inside the combustion chamber and thus improve performance, emissions, and combustion characteristics [23, 31]. The physical optimization of engine parameters is an expensive and time-consuming process. To address the issue CFD concepts are used in the optimization of IC engine parameters. The formation of mixtures within the combustion chamber is the most significant aspect in deciding the quality of combustion [5, 45]. The optimization of mixture formation is primarily dependent on the tendency of the combustion chamber geometry to induce turbulent kinetic energy (TKE) inside the combustion chamber [26]. [7] used the commercial software CONVERGE CFD to examine the flow pattern corresponding to different piston geometries and concluded that the bowl piston geometry is preferred over the creviced piston geometry for increasing turbulence inside the combustion chamber. [8] examined the various shape combustion chambers, namely hemispherical combustion chamber (HCC), shallow depth combustion chamber (SCC), and toroidal combustion chamber (TCC), and discovered that the TCC provides a better homogeneous mixture of air and fuel, resulting in better performance, emission, and combustion characteristics in the CI engine. [27] investigated numerically and experimentally the effect of tangential holes in the piston crown, with diameters of 2, 2.5, 3, and 3.5 mm and discovered that the air motion inside the piston cavity is improved compared to the unmodified piston; the better air movement inside the combustion chamber provides an opportunity to reduce HC, CO, and soot emissions. [16] investigated a CI engine fueled by methyl ester of pumpkin seed oil and Moringa oleifera oil with various modified piston bowls. The results show that the toroidal combustion chamber provides superior performance, emission, and combustion characteristics. [18] used the commercial code AVL FIRE CFD to simulate the in-cylinder flow and combustion of various spray angles and combustion chamber profiles. The numerical simulation demonstrates that the toroidal reentrant combustion chamber outperforms other combustion chamber profiles. [39] used STAR-CD CFD software to simulate a diesel engine fueled by natural gas and diesel in dual fuel mode with three different diesel spray-oriented piston geometries and radial clearances. The simulation results show that all of the modified piston geometries enhanced TKE than the unmodified piston.

From the above literature review it becomes clear that biodiesel can be an alternative and can be used along with conventional gaseous fuel like acetylene in the CI engine in order to obtain clean combustion and improved performance. Furthermore, most studies have focused on the modification of piston profiles to enhance the performance, emission, and combustion characteristics of CI engines, and have concluded that the toroidal piston profile generates more TKE due to high swirl and squish behavior. Very few works in the literature concern the effect of holes in the piston. According to the author's knowledge, there is no experimental or numerical research available for a dual fuel engine fueled by mahua biodiesel and acetylene gas utilizing a toroidal piston profile carrying helical holes in the crown surface to attain improved performance, emission, and combustion characteristics. In order to fill the research gap, the present work focuses on the numerical investigation on the CI engine fueled either by diesel with 3 LPM acetylene or B20 mahua biodiesel with 3 LPM of acetylene gas in dual fuel operation. The current

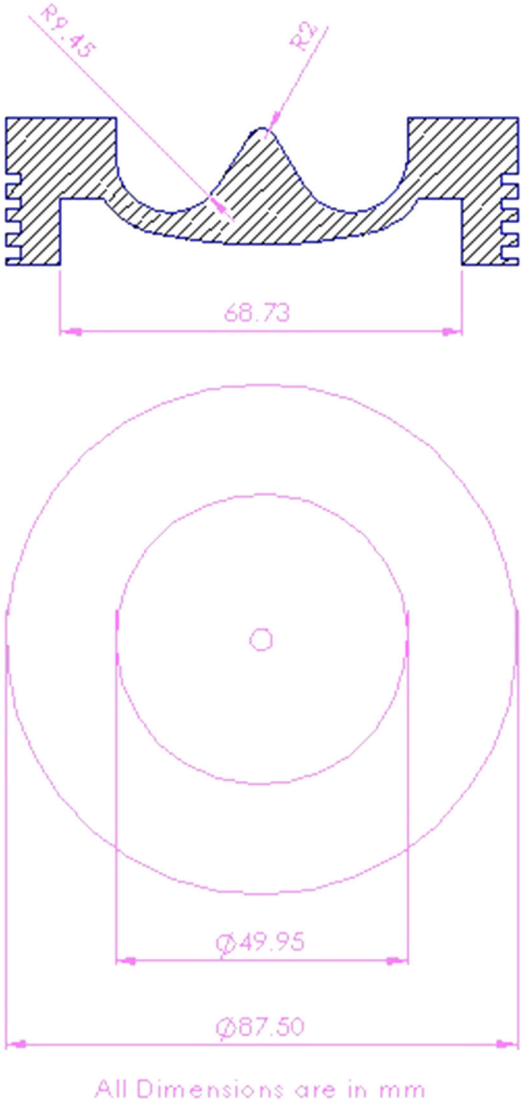

Fig. 1 Toroidal Piston Profile

study is carried out in two phases. The first phase consists of determining the optimized piston bowl geometry using diesel with 3 LPM acetylene gas fuel. The second phase involves determining the optimized piston bowl geometry, which is fueled by B20 mahua biodiesel with 3 LPM acetylene gas. The optimization of piston bowl geometry is carried out by means of analyzing the CFD results of turbulent intensity and turbulent kinetic energy inside the combustion chamber.

2 Design of Piston Bowl Geometry

The 3-D model of the toroidal piston with helical holes of varying diameter and count was created with the CAD software SOLIDWORKS. The existing unmodified toroidal piston profile is shown in Fig. 1. There are totally nine different piston geometries that are modeled using SOLIDWORKS software. The piston geometry is modeled in such a way that 1-mm holes with counts of 3, 4, and 5 appear on the surface of the piston crown. Similarly, 1.5- and 2-mm-diameter holes with counts of 3, 4, and 5 were modeled. In case of 3, 4, and 5 holes, the holes are separated by the angular distance of 120°, 90°, and 72°, respectively. The inclination of each helical hole toward the piston central cavity is 80° to the horizontal plane and 40° to the vertical plane in order to improve turbulence inside the combustion chamber. Figures 2, 3, and 4 represent the plan of a CAD-modeled piston with holes of 1, 1.5, and 2 mm diameter and three different counts (3, 4 and 5).

The toroidal combustion chamber is ideal for improved performance at high speed engine. The toroidal piston profile achieves better performance than conventional piston profiles due to higher in-cylinder swirl and TKE [28]. The net volume of the combustion chamber for various piston geometries is shown in Table 1; according to it, the cubic capacity slightly varies and thus the compression ratio does not change.

3 CFD Model

The multidimensional CFD simulations were carried out by finite volume-based ANSYS-FLUENT CFD code and refers to the time interval from the start of the fuel injection (SFI) to the end of the fuel injection (EFI). The fuel injection starts at 5° bTDC and ends at 25° aTDC.

3.1 Governing Equations

The equations that govern gas dynamics are terminology of conservation and thermodynamic laws. The simulation is based on a non-stationary 3D turbulence model. Gases are characterized as compressible viscous fluids. To solve flow problems inside cylinder configurations, the standard model k-ε (Turbulent Kinetic Energy-Turbulence Dissipation Rate) is used. The governing equations the inflow model, such as momentum conservation, mass conservation and energy conservation, are summed up in conservative form in the Reynolds-averaged Navier–Stokes (RANS) equations.

The following equations govern the gas phase and can be written in the conservation form.

$$\frac{\partial \rho}{\partial t} + \frac{\partial}{\partial x_i}(\rho u_{\mathrm{i}}) = 0 \tag{1}$$

[29]

$$\frac{\partial}{\partial t}(\rho u_{\mathrm{i}}) + \frac{\partial}{\partial x_{\mathrm{i}}}(\rho u_{\mathrm{i}} u_{\mathrm{j}}) + \frac{\partial p}{\partial x_{\mathrm{i}}} = \frac{\partial}{\partial x_{\mathrm{i}}}\left(\tau_{\mathrm{ij}} + \tau_{\mathrm{ij}}^{\mathrm{R}}\right) + S_{\mathrm{i}};\ i = 1, 2, 3 \tag{2}$$

[40]

$$\frac{\partial \rho H}{\partial t} + \frac{\partial \rho u_{\mathrm{i}} H}{\partial x_{\mathrm{i}}} = \frac{\partial}{\partial x_{\mathrm{i}}}\left(u_{\mathrm{j}}\left(\tau_{\mathrm{ij}} + \tau_{\mathrm{ij}}^{\mathrm{R}}\right) + q_{\mathrm{i}}\right) + \frac{\partial \rho}{\partial t} - \tau_{\mathrm{ij}}^{\mathrm{R}}\frac{\partial u_{\mathrm{i}}}{\partial x_{\mathrm{j}}} + \rho\varepsilon + S_{\mathrm{i}}u_{\mathrm{i}} + Q_{\mathrm{H}} \tag{3}$$

where $H = h + \frac{u^2}{2}$ [13].

Subscripts are used to represent summation across the three coordinate directions.

The energy equation is given in Eq. (4)

$$\frac{\partial \rho E}{\partial t} + \frac{\partial \rho u_{\mathrm{i}}\left(E + \frac{p}{\rho}\right)}{\partial x_{\mathrm{i}}} = \frac{\partial}{\partial x_{\mathrm{i}}}\left(u_{\mathrm{j}}\left(\tau_{\mathrm{ij}} + \tau_{\mathrm{ij}}^{\mathrm{R}}\right) + q_{\mathrm{i}}\right) - \tau_{\mathrm{ij}}^{\mathrm{R}}\frac{\partial u_{\mathrm{i}}}{\partial x_{\mathrm{j}}} + \rho\varepsilon + S_{\mathrm{i}}u_{\mathrm{i}} + Q_{\mathrm{H}} \tag{4}$$

where $E = e + \frac{u^2}{2}$ [15].

3.2 Turbulence Model

In order to predict the turbulence generation inside the combustion chamber, the Re-Normalized Group (RNG) variant of k-ε turbulence model was adopted. The governing equations are,

$$\frac{\partial}{\partial t}(\rho k) + \frac{\partial}{\partial x_{\mathrm{i}}}(\rho k u_{\mathrm{i}}) = \frac{\partial}{\partial x_{\mathrm{j}}}\left\{\left(\mu + \frac{\mu_{\mathrm{t}}}{\sigma_{\mathrm{k}}}\right)\frac{\partial k}{\partial x_{\mathrm{j}}}\right\} + P_{\mathrm{k}} - \rho\varepsilon \tag{5}$$

[10]

$$\frac{\partial}{\partial t}(\rho\varepsilon) + \frac{\partial}{\partial x_{\mathrm{i}}}(\rho\varepsilon u_{\mathrm{i}}) = \frac{\partial}{\partial x_{\mathrm{j}}}\left\{\left(\mu + \frac{\mu_{\mathrm{t}}}{\sigma_{\varepsilon}}\right)\frac{\partial \varepsilon}{\partial x_{\mathrm{j}}}\right\} + C_{1\varepsilon}\frac{\varepsilon}{k}P_{\mathrm{k}} - C_{2\varepsilon}^{*}\rho\frac{\varepsilon^2}{k} \tag{6}$$

[10]

The RNG k-ε model was used to account for the turbulence of fluid motion within the closed volume [21]. The

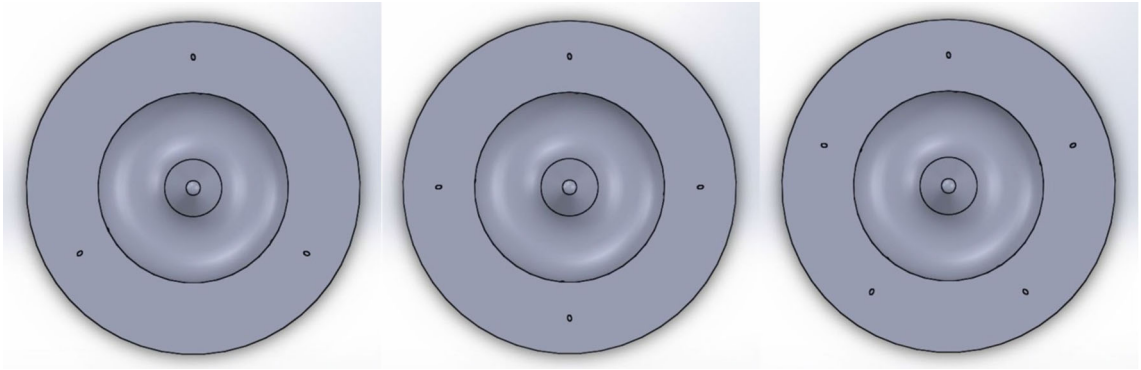

Fig. 2 CAD view of 1-mm-diameter hole with the hole count of 3, 4, and 5

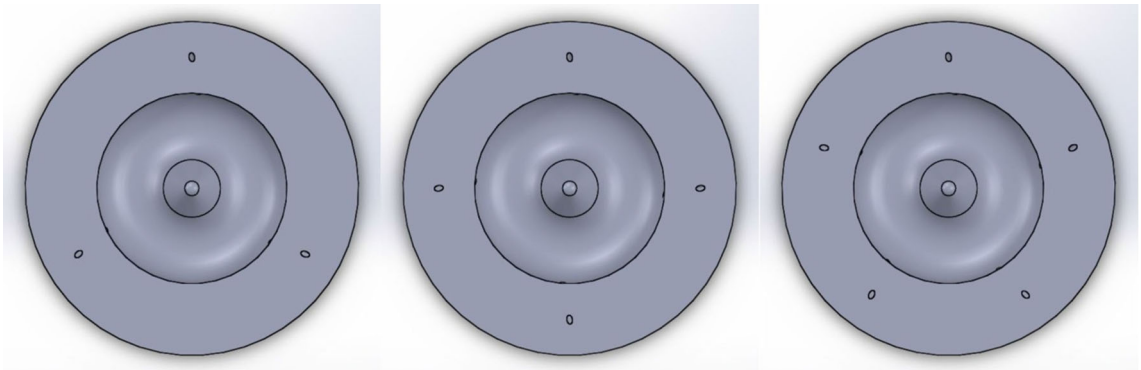

Fig. 3 CAD view of 1.5-mm-diameter hole with the hole count of 3, 4, and 5

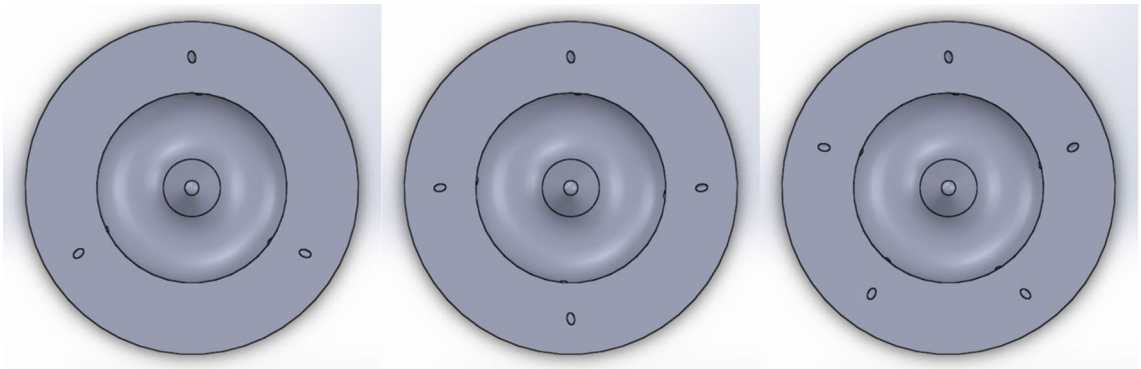

Fig. 4 CAD view of 2-mm-diameter hole with the hole count of 3, 4, and 5

simulation was performed with the assumption that no heat transfer occurs in between the cylinder wall and the piston. Table 2 summarizes the engine specifications used for the CFD simulation.

3.3 Droplet Breakup Model

The bagging and stripping of aerodynamic forces are considered to be the cause of droplet breakup. A non-uniform pressure gradient around the fuel droplet is thought to induce instability in the bag breakup [32]. A spray of liquid fuel droplets is injected into the stream of air where the combustion takes place, followed by the evaporation of these droplets and the reaction of the gaseous (vapor) fuel with the oxidant. Convective heat transfer mechanisms, which range from 100 to 500 W/m^2 K depending on the flow velocity, are used in the evaporation process. The instability is determined by a critical value of the Weber number. The breakup rate is determined based on the following equation.

$$\frac{\mathrm{d}D_\mathrm{d}}{dt} = \frac{\left(D_\mathrm{d} - D_\mathrm{d,stable}\right)}{t_\mathrm{b}} \tag{7}$$

Table 1 Combustion Chamber Volume for piston geometries

Piston geometry	Cubic capacity in mm^3
Unmodified Piston	661,452.5
1 mm 3 holes	661,482.1
1 mm 4 holes	661,490.1
1 mm 5 holes	661,492.2
1.5 mm 3 holes	661,519.1
1.5 mm 4 holes	661,541.7
1.5 mm 5 holes	661,564.3
2 mm 3 holes	661,572.1
2 mm 4 holes	661,612.4
2 mm 5 holes	661,652.4

Table 2 Engine specification for CFD simulation

Type	Vertical inline diesel, four-stroke, water-cooled engine
No of cylinder	Single cylinder
Stroke, Bore	110, 87.5 mm
Compression ratio	17.5:1
Crank radius	55 mm
Connecting rod length	234 mm
Brake power	5.2 kW
Speed	1500 rpm
İnjection hole diameter	0.28 mm
No. of holes	3
Injection pressure	220 bar
Start of fuel injection (SFI)	5° bTDC
End of the fuel injection (EFI)	25° aTDC

[32] where D_d is the instantaneous droplet diameter, $D_{d,stable}$ is stable droplet diameter, and t_b is the characteristics time scale.

3.4 Droplet Wall Interaction MODEL

A stochastic approach is used to calculate various post impingement quantities of the droplet in order to reflect the dynamic characteristics of the impingement process. Droplet rebound is more common when the temperature of the wall exceeds the liquid Leiden frost temperature. As the kinetic energy of the incident drop and the surface temperature rise, the mass of the secondary drop will grow [52]. This model allows for a distribution of sizes and velocities in the secondary droplet that results from the initial droplet slash [2, 41]. It generates a variety of impingement regimes based on a number of variables, including incident droplet velocity relative to the wall, incident angle, droplet size and characteristics, wall temperature, wall surface roughness, liquid layer thickness, and near-wall gas conditions.

3.5 Atomization Model

The atomization model is based on the gas inertia and the initial turbulence stress generated in the nozzle, which are the two most fundamental factors in spray atomization. The turbulence created in the nozzle hole causes early disturbances on the jet's surface as it exits the hole. Once the perturbations have attained a particular threshold, the pressure force caused by the interaction with the surrounding gas causes them to increase exponentially, until the perturbation become separated from the jet surface as droplets [Huh 14]. Liquid fuel droplets will completely vaporize before the combustion process begins for small liquid fuel droplets. The diffusion of the fuel vapor into the air or gas-to-gas mixing then controls the combustion rate. As a result, good physical gas-to-gas mixing will disrupt the diffusion-controlled mechanism. This will increase the overall rate of combustion. The average TKE (k) and its dissipation rate (ε), at the exit of the nozzle hole, are calculated from Eqs. (8) and (9), respectively.

$$k_a = \frac{U^2}{8L/D}\left(\frac{1}{c_d^2} - K_c - 1\right) \tag{8}$$

[14]

$$\varepsilon_a = \frac{K_\varepsilon U^3}{2L}\left(\frac{1}{c_d^2} - K_c - 1\right) \tag{9}$$

[14] where U is the average injection velocity over the time of injection and L and K_c are the hole length and form loss coefficient, respectively. K_ε is an empirical coefficient and c_d is the discharge coefficient of the nozzle.

3.6 Initial Boundary conditions

The ambient pressure and temperature are taken at the start of the suction stroke (1 bar and 300 K). The mixing length scale is set to 0.001 m and the turbulence intensity is set to 5%. The attach boundary conditions which include engine parameters such as crank shaft speed, starting and ending crank angle, crank angle step size is utilized to connect valve and cylinder regions during the opening and closing periods for valves. Appropriate temperature values for the wall boundary conditions are specified in combination, with no slip condition. Table 2 shows the engine operating boundary conditions used for engine simulation, whereas Table 3 shows the properties of different fuels used in the simulations.

3.7 CFD Model Validation

In this study, the different piston geometries were modeled with intake valve supplying air and 3 LPM acetylene gas. The RNG k-ε turbulence model was employed and solid cone

Table 3 Fuel properties for simulation

Properties	Diesel	B20 Mahua	Acetylene fluid	Air fluid
Molecular weight (kg/kg^{-mol})	142.32	194.0785	26.04	28.966
Density (kg/m^3)	825	831	1.092	1.225
Thermal conductivity (W/m^{-k})	0.13	–	0.0213	0.0242
Viscosity (kg/m-s)	2.145*10^{-03}	3*10^{-03}	1*10^{-05}	1.7894*10^{-05}

shaped 3-hole diesel injector were used. The results of the simulation at 1500 rpm and full load were compared with prior simulation and experimental work by [16]. The problem described by [16] was solved using the present-study model (RNG k-ε turbulence model). The TKE variations for the unmodified piston are clearly in good agreement with previous work. On the basis of the validated model, the effects of piston shape and fuel type (diesel or biodiesel) on turbulence intensity and TKE were simulated.

3.8 Mesh Independence Study

Accuracy of the CFD simulation is greatly influenced by mesh size so grid-independent study is required. This concerns the task to find the minimum number of cells required for the results to converge from the subsequent cell quantity. In the present work, 5 mesh sizes were used, consisting of 150,000, 200,000, 221,600, 250,000, and 300,000 tetrahedral cells. Figure 5 shows the TKE variation along the mean line on the symmetry plane for 1 mm diameter with 5 holes piston geometry fueled by diesel with 3 LPM acetylene gas at different mesh size. At the 221,600 tetrahedral cell quantity, the results are convergent with the 250,000 and 300,000 tetrahedral cell quantity. It is therefore concluded that the mesh size 221,600 is sufficient for attain accurate simulation results. Figure 6 shows the mesh domain for the modified piston bowl.

4 Results and Discussion

The CFD simulations were performed in two phases. The first phase of the simulation work involved determining the optimum number of holes required for producing enough turbulence in the combustion chamber, based on the percentage of turbulent intensity generated. The second phase involved determining the optimum diameter of the hole required to produce swirl inside the combustion chamber, based on the turbulent kinetic energy generated. For all the simulations, the engine was run at a fixed speed of 1500 rpm, virtually. To obtain precise results and to reduce the required system memory and time, each simulation started at a crank angle of 5° bTDC to 25° aTDC. At these crank angles turbulence in the combustion chamber is high due to start and end of fuel injection [37]. Prior to the start of the simulation work, the combustion chamber was considered to be filled with intake air and acetylene gas. The in-cylinder flow motion is mainly driven by the upward-moving piston in compression stroke from the intake valve close (IVC), at which the turbulence is relatively very small and can be ignored. Thus, a simulation from IVC was more reliable. All the governing equations including Reynolds-averaged Navier–Stokes (RANS) equation, Re-Normalized Group (RNG) variant of k-ε turbulence model, droplet breakup model, droplet wall interaction model, Atomization model are solved using FLUENT module which is contained in it.

4.1 Parametric Study of Number of Holes in Piston

For achieving higher thermal efficiency and minimal amount of pollutant, it is required to increase the flame speed inside the combustion chamber, in order to eradicate the negative impact of biofuels and gaseous fuels. The high flame speed ignites end gas quickly and grasps the fuel energy in a shorter period of time, avoiding detonation. The speed of flame propagation is affected by the amount of turbulent intensity inside the combustion chamber [22]. Depending on the piston bowl geometry, the turbulence intensity does not generally vary during the suction stroke, but it does vary at compression stroke ending and during the combustion. As a result, the percentage of turbulent intensity developing inside the combustion chamber has be calculated, specifically at compression stroke ending and during the combustion stage.

The variation in turbulence intensity within the combustion chamber affects the tendency of fuel homogeneous mixture formation, particularly in dual fuel combustion [4]. The higher the degree of homogeneous mixture formation, the better the engine performance, emission, and combustion characteristics compared to fuels with a low degree of homogeneous mixture formation [24]. Figures 7 and 8 illustrate the turbulent intensity distribution contours along the mean line on the symmetry plane in modified piston geometries with 3, 4, and 5 holes with diameters of 1, 1.5, and 2 mm, and fueled by diesel with 3 LPM acetylene and B20 mahua with 3 LPM acetylene, respectively. The turbulence intensity is defined by the ratio of velocity fluctuations root mean square to mean flow velocity. The highest turbulent intensity at the central plane of the combustion chamber for

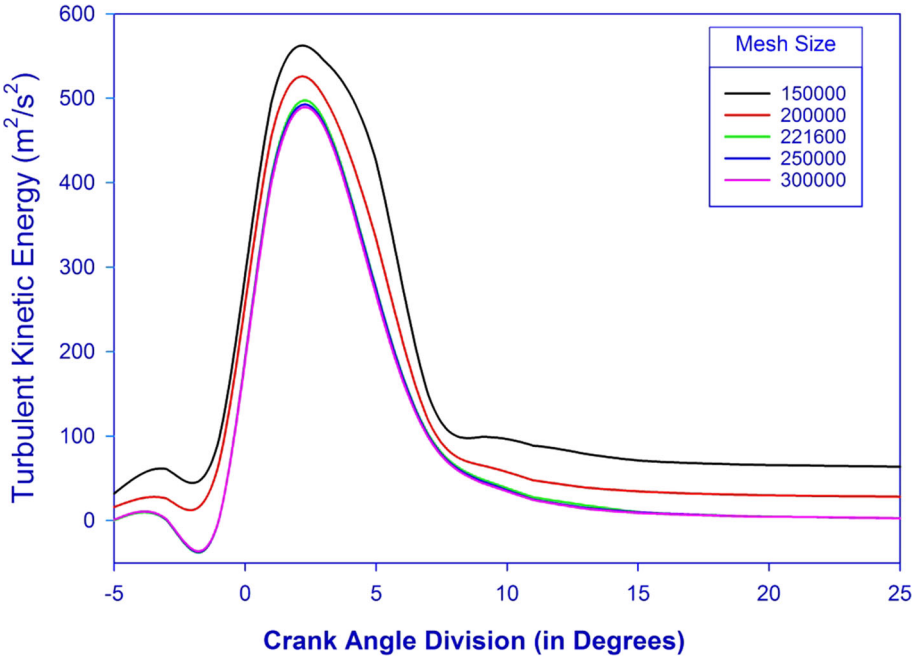

Fig. 5 TKE variation along the mean line on the symmetry plane for 1 mm diameter with 5-hole- piston geometry fueled by diesel with 3 LPM acetylene gas at different mesh size

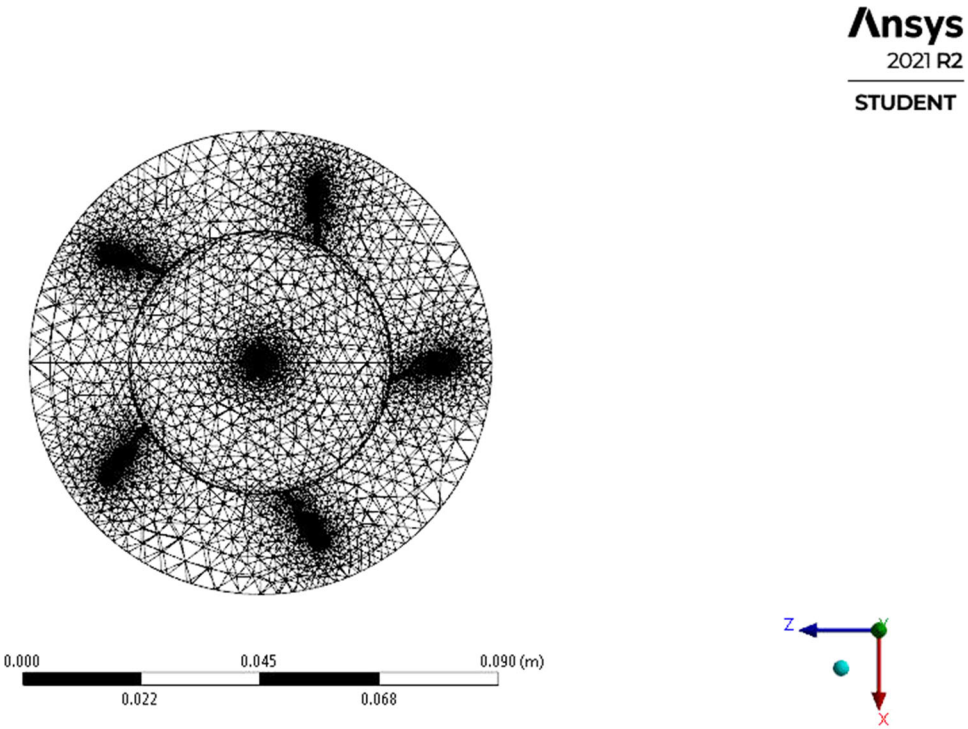

Fig. 6 Mesh domain of the piston bowl for CFD simulation

diesel with 3 LPM acetylene gas injection is 40.87%, and it has been predicted in the modified piston with 5 holes of 1 mm diameter.

Figure 9 represents the turbulent intensity variation graph at the symmetry plane for the various piston geometries in case of using diesel with acetylene mixture. Modified pistons with 3 and 4 holes, all with the same diameter range, produce the same level of turbulent intensity, whereas the 5 hole cases with hole diameters of 1 and 2 mm generate the higher amount of turbulent intensity. The higher turbulent intensity is caused by the higher number of holes in the piston; these create a higher velocity difference in the piston cavity and piston crown regions, compared to pistons with fewer holes. Moreover, the smaller diameter holes produce an orifice effect, increasing the velocity of the diesel fuel particles. The maximum turbulent intensity at the central plane

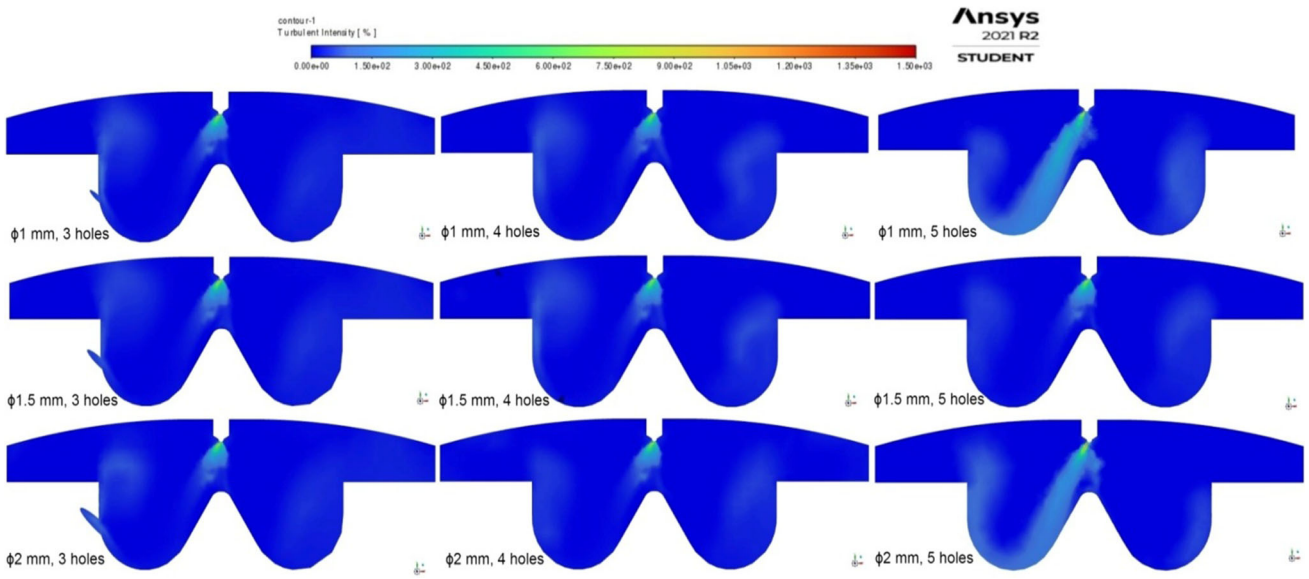

Fig. 7 Contours of turbulent intensity distribution for modified piston bowl fueled by diesel and 3 LPM acetylene along the mean line on the symmetry plane

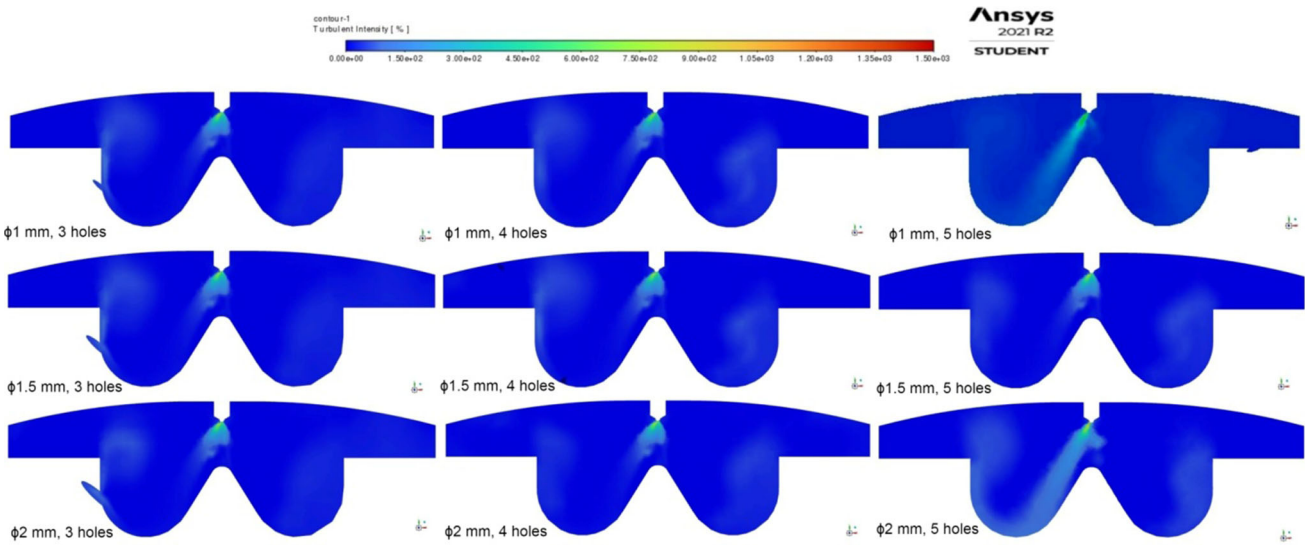

Fig. 8 Contours of turbulent intensity distribution for modified piston bowl fueled by biodiesel and 3 LPM acetylene along the mean line on the symmetry plane

of the combustion chamber for B20 mahua biodiesel in the modified piston of 5 holes of 2-mm-diameter piston geometry is 36.69%. Except for the 5 holes with 1 mm and 2 mm diameter, the turbulent intensity contours and turbulent intensity variation graph for the modified piston geometries fueled by biodiesel are the same as for the diesel fueled operation (Fig. 10). The maximum turbulent intensity is predicted in the geometry with 5 holes of 2-mm-diameter piston rather than the 1-mm-diameter hole. This is because the density of the B20 mahua biodiesel is greater than the density of diesel, so fuel particles pass more freely and through 2 mm hole compared to the case of 1 mm diameter where the part of the fuel particles will stick due its higher density.

The turbulent intensity contours also show that the velocity fluctuation for the B20 mahua biodiesel fueled operation at the injection area in the combustion chamber is higher than for the diesel operation [11]. However, the diesel-fueled combustion generates more turbulent intensity in the combustion chamber. The variation in turbulent intensity in biodiesel is caused by the higher density of the biodiesel particles entering the combustion chamber with higher velocity due to self-weight. But even so, the velocity fluctuation of subsequent particles is adversely reduced because the time span

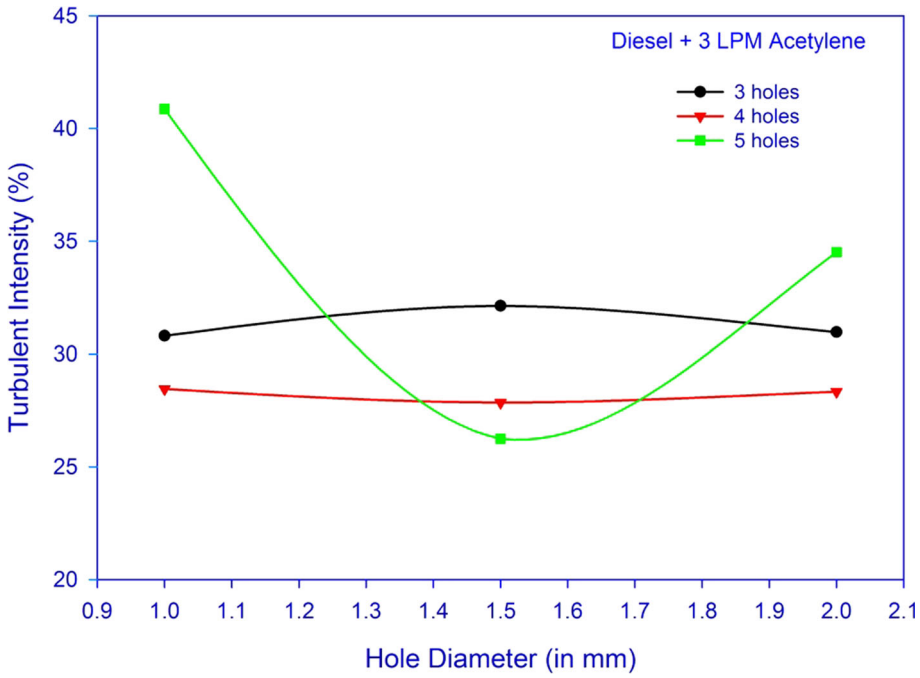

Fig. 9 Comparison graph of turbulent intensity variation for different piston bowl geometry fueled by diesel and 3 LPM acetylene along the mean line on the symmetry plane

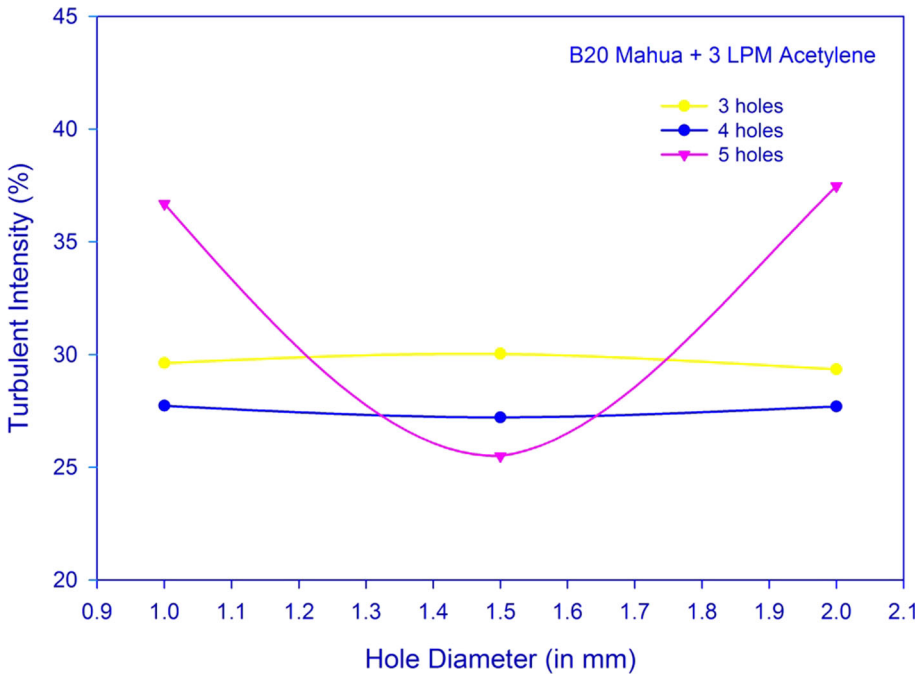

Fig. 10 Comparison graph of turbulent intensity variation for different piston bowl geometry fueled by B20 Mahua and 3 LPM acetylene along the mean line on the symmetry plane

of homogeneous mixture formation with acetylene gas is comparatively longer than that of diesel fuel. The turbulent intensity is higher at the combustion chamber hitting region only due to this velocity fluctuation. Due to the lower density of the fuel, the velocity fluctuations at the time of the collision are low for diesel. Moreover, the subsequent diesel fuel particle velocity fluctuation is greater because the time span of homogeneous mixture formation with acetylene gas is less than that of the biodiesel fueled operation [7]. Because of this fuel particle behavior, the turbulent intensity of the diesel with 3 LPM acetylene gas at the central plane of the combustion chamber is greater than the B20 Mahua biodiesel operation with 3 LPM acetylene gas in all of the modified piston geometries.

4.2 Parametric Study of Hole Diameter

Whenever the turbulent intensity and TKE for the piston geometries increase, the combustion duration decreases, resulting in enhanced performance and emission character-

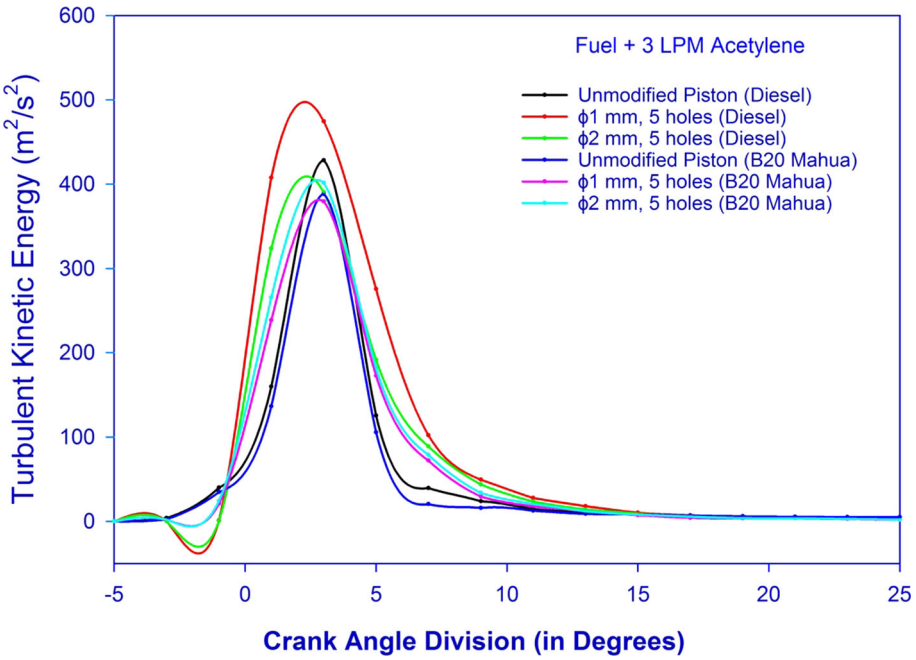

Fig. 11 TKE variation for unmodified and modified piston geometry fueled by diesel and B20 mahua with 3 LPM acetylene along the mean line on the symmetry plane

istics [50]. According to the turbulent intensity distribution contours and the turbulent intensity graph, the piston geometry with 5 holes produces comparatively higher turbulent intensity, especially with hole diameters of 1 mm and 2 mm for both diesel and B20 Mahua biodiesel with 3 LPM acetylene gas fueled operation. In order to optimize the diameter of hole which can produce better turbulence inside the combustion chamber, it is required to find the TKE variation across the crank angle from the SFI (5° bTDC) to the EFI (25° aTDC).

Figure 11 shows the TKE variation for unmodified and modified piston geometry fueled by diesel and B20 mahua with 3 LPM acetylene. The graph shows that the TKE inside the combustion chamber for the modified piston geometries fueled by both diesel and biodiesel is less than that of unmodified piston at SFI. This is because the fuel passes through the helical holes without causing turbulence with the in-cylinder air and acetylene mixture at the start of the crank movement. The unmodified piston, on the other hand, creates turbulence with the in-cylinder air and acetylene mixture during the initial stage of the crank movement. The modified piston geometry of 1 mm diameter with 5 holes fueled by diesel with 3 LPM acetylene gas in dual fuel operation achieving higher TKE than the other piston and fuel configurations. The reason behind this higher TKE is when the piston reaches TDC, the fuel charge enters the squish region with high velocity, creating more turbulence than with the other piston geometry. This high turbulence fuel mixture creates even more turbulence with freshly injected fuel through the injector, allowing it to reach peak TKE earlier than the unmodified piston geometry.

For the B20 mahua in dual fuel operation, the piston movements up to top dead center, as well as the TKE distribution trend, are similar to those seen in diesel-fueled operations. The modified piston geometry of 2 mm diameter with 5 holes, on the other hand, exhibits the highest TKE, which is comparatively similar to unmodified piston with diesel-fueled operation. The possible reason is, after reaching the piston in to the TDC, the B20 mahua biodiesel particles tends to go squish region through the holes. Because of the density of B20 mahua biodiesel, the fluid particle size is larger than diesel. As a result, a B20 mahua biodiesel fueled operation necessarily requires a larger hole diameter to facilitate flow through the helical holes. It can also be observed that the peak TKE for modified piston geometries is not much advanced compared to diesel-fueled operation because when the B20 mahua biodiesel particles make contact with the combustion chamber walls, the velocity drops due to the higher mass of the fuel particle.

5 Conclusion

In the present numerical study, nine piston geometries with 3, 4, and 5 holes of diameter 1, 1.5, or 2 mm with the helical hole counts of 3, 4, and 5 are investigated in order to find out the ones that enhance turbulence generation when fueled by diesel and 3 LPM acetylene gas and B20 mahua biodiesel and 3 LPM acetylene gas in dual fuel mode using ANSYS FLUENT CFD software. From the simulation results the following conclusions are drawn.

The piston geometry with 5 hole counts and diameters of 1 mm fueled by diesel in dual fuel mode having a turbulent intensity of 40.87% which is higher than the all other piston geometries due to their higher velocity fluctuation generating ability. The peak TKE value of 474.48 m^2/s^2 is observed at the optimum piston geometry of 1 mm diameter with 5 holes as the diesel and 3 LPM acetylene gas in dual fuel mode, whereas the piston geometry with 5 hole counts and diameters of 2 mm fueled by B20 mahua biodiesel in dual fuel mode having a turbulent intensity of 37.48% and its corresponding TKE value is 401.48 m^2/s^2, which is higher than the any other piston geometries fueled by B20 mahua in dual fuel operation. Furthermore, the best piston geometry of 2 mm in diameter with 5 holes fueled by B20 mahua biodiesel dual fuel mode TKE value is comparable with the unmodified piston with diesel in dual fuel operation has a TKE value of 428.36 m^2/s^2. To grasp the advantage of environment friendly biodiesel fueled operation without compromising the performance can be achieved by modifying the piston by making 5 holes with 2 mm in diameter preferred.

The future scope of the work is based on the CFD simulation results; physically modifying the piston geometry and conducting numerical experiments to attain improved performance, emission, and combustion characteristics.

Authors Contributions G. Babusankar carried out the design of the work and Data collection; V. Manieniyan has done the data analysis, interpretation and drafting of the article; S. Sivaprakasam was involved in the critical revision of the article and Final approval of the version to be published.

References

1. Akkoli, K.M.; Banapurmath, N.R.; Shivashimpi, M.M.; Soudagar, M.E.M.; Badruddin, I.A.; Alazwari, M.A.; Venu, H.: Effect of injection parameters and producer gas derived from redgram stalk on the performance and emission characteristics of a diesel engine. Alex. Eng. J. **60**(3), 3133–3142 (2021)
2. Bai, C.,; Gosman, A. D: Development of methodology for spray impingement simulation. SAE Trans., 550–568 (1995)
3. Banapurmath, N.R.; Chandrashekar, T.K.; Soudagar, M.E.M.; Anqi, A.E.; Mujtaba, M.A.; Goodarzi, M.; Ali, M.A.: Effect of parameters behavior of simarouba methyl ester operated diesel engine. Energies **14**(16), 4973 (2021)
4. Bari, S.; Hossain, S.N.; Saad, I.: A review on improving airflow characteristics inside the combustion chamber of CI engines to improve the performance with higher viscous biofuels. Fuel **264**, 116769 (2020)
5. Chiodi, M.; Berner, H. J.; Bargende, M.: Investigation on mixture formation and combustion process in a CNG-engine by using a fast response 3D-CFD-simulation (No. 2004–01–3004). SAE Technical Paper, (2004)
6. Dasrath, D.K.; Biwalkar, R.; Singh, S.; Northrop, W.F.: Bowl piston geometry as an alternative to enlarged crevice pistons for rapid compression machines. Proc. Combust. Inst. **38**(4), 5723–5731 (2021)
7. Deivajothi, P.; Manieniyan, V.; Sivaprakasam, S.: An impact of ethyl esters of groundnut acid oil (vegetable oil refinery waste) used as emerging fuel in DI diesel engine. Alex. Eng. J. **57**(4), 2215–2223 (2018)
8. Ganji, P.R.; Singh, R.N.; Raju, V.R.K.; Rao, S.S.: Design of piston bowl geometry for better combustion in direct-injection compression ignition engine. Sādhanā **43**(6), 1–9 (2018)
9. Ge, S.; Brindhadevi, K.; Xia, C.; Elesawy, B.H.; Elfasakhany, A.; Unpaprom, Y.; Van Doan, H.: Egg shell catalyst and chicken waste biodiesel blends for improved performance, combustion and emission characteristics. Fuel **306**, 121633 (2021)
10. Han, Z.; Reitz, R.D.: Turbulence modeling of internal combustion engines using RNG κ-ε models. Combust. Sci. Technol. **106**(4–6), 267–295 (1995)
11. Hara, S.; Tsukahara, T.; Kawaguchi, Y.: Experimental investigation of streamwise velocity fluctuation based on the Reynolds-number dependency in turbulent viscoelastic-fluid flow. Int. J. Heat Fluid Flow **68**, 281–289 (2017)
12. Harari, P.A.; Banapurmath, N.R.; Yaliwal, V.S.; Soudagar, M.E.M.; Khan, T.Y.; Mujtaba, M.A.; EL-Seesy, A.I.: Experimental investigation on compression ignition engine powered with pentanol and thevetia peruviana methyl ester under reactivity controlled compression ignition mode of operation. Case Stud. Therm. Eng. **25**, 100921 (2021)
13. Heywood, J. G. Viscous incompressible fluids: mathematical theory (2006)
14. Huh, K. Y. (1991). A phenomenological model of diesel spray atomization. In *Proc. of The International Conf. on Multiphase Flows' 91-Tsukuba*
15. Jemni, M.A.; Kantchev, G.; Abid, M.S.: Influence of intake manifold design on in-cylinder flow and engine performances in a bus diesel engine converted to LPG gas fuelled, using CFD analyses and experimental investigations. Energy **36**(5), 2701–2715 (2011)
16. Karthickeyan, V.: Effect of combustion chamber bowl geometry modification on engine performance, combustion and emission characteristics of biodiesel fuelled diesel engine with its energy and exergy analysis. Energy **176**, 830–852 (2019)
17. Khan, H.; Soudagar, M.E.M.; Kumar, R.H.; Safaei, M.R.; Farooq, M.; Khidmatgar, A.; Taqui, S.N.: Effect of nano-graphene oxide and n-butanol fuel additives blended with diesel–Nigella sativa biodiesel fuel emulsion on diesel engine characteristics. Symmetry **12**(6), 961 (2020)
18. Khan, S.; Panua, R.; Bose, P.K.: Combined effects of piston bowl geometry and spray pattern on mixing, combustion and emissions of a diesel engine: a numerical approach. Fuel **225**, 203–217 (2018)
19. Kumar, M.V.; Babu, A.V.; Kumar, P.R.: Experimental investigation on the effects of diesel and mahua biodiesel blended fuel in direct injection diesel engine modified by nozzle orifice diameters. Renew. Energy **119**, 388–399 (2018)
20. Lakshmanan, T.; Nagarajan, G.: Experimental investigation on dual fuel operation of acetylene in a DI diesel engine. Fuel Process. Technol. **91**(5), 496–503 (2010)
21. Miles, P.; Megerle, M.; Hammer, J.; Nagel, Z.; Reitz, R. D.; Sick, V.: Late-cycle turbulence generation in swirl-supported, direct-injection diesel engines. SAE Trans. 1510–1529 (2002)
22. Montoya, J.P.G.; Arrieta, A.A.A.: Effect of the turbulence intensity on knocking tendency in a SI engine with high compression ratio using biogas and blends with natural gas, propane and hydrogen. Int. J. Hydrogen Energy **44**(33), 18532–18544 (2019)
23. Muthuswamy, S.; Veerasigamani, M.:Impact of secondary fuel injector in various distance on direct injection diesel engine using acetylene-bio diesel in reactivity controlled compression ignition mode. Energy Sour. Part A Recovery Util. Environ. Effects, 1–15 (2020)
24. Muthuswamy, S.; Veerasigamani, M; Comparative experimental analysis on dual fuel with biodiesel-acetylene in reactivity controlled compression ignition engine. Int. J. Ambient Energy, 1–12 (2021)

25. Oni, B.A.; Sanni, S.E.; Daramola, M.; Olawepo, A.V.: Effects of oxy-acetylation on performance, combustion and emission characteristics of Botryococcus braunii microalgae biodiesel-fuelled CI engines. Fuel **296**, 120675 (2021)
26. Prabhakaran, P.; Ramesh, P.; Saravanan, C.G.; Loganathan, M.; Gunasekaran, E.J.: Experimental and numerical investigation of swirl enhancing grooves on the flow and combustion characteristics of a DI diesel engine. Energy **115**, 1234–1245 (2016)
27. Prabhakaran, P.; Saravanan, C.G.; Vallinayagam, R.; Vikneswaran, M.; Muthukumaran, N.; Ashok, K.: Investigation of swirl induced piston on the engine characteristics of a biodiesel fueled diesel engine. Fuel **279**, 118503 (2020)
28. Prasad, B.V.V.S.U.; Sharma, C.S.; Anand, T.N.C.; Ravikrishna, R.V.: High swirl-inducing piston bowls in small diesel engines for emission reduction. Appl. Energy **88**(7), 2355–2367 (2011)
29. Rahmanian, B.; Safaei, M.R.; Kazi, S.N.; Ahmadi, G.; Oztop, H.F.; Vafai, K.: Investigation of pollutant reduction by simulation of turbulent non-premixed pulverized coal combustion. Appl. Therm. Eng. **73**(1), 1222–1235 (2014)
30. Rajak, U.; Nashine, P.; Dasore, A.; Verma, T. N.: Utilization of renewable and sustainable microalgae biodiesel for reducing the engine emissions in a diesel engine. Fuel, 122498 (2021)
31. Ranganatha Swamy, L.; Banapurmath, N. R.; Chandrashekar, T. K.; Soudagar, M. E. M.; Gul, M.; Nik-Ghazali, N. N.; Goodarzi, M.: Effect of injection timing and duration on the performance of diesel engine fueled with port injection of oxygenated fuels.Chem. Eng. Commun., 1–13 (2021)
32. Reitz, R. D., & Diwakar, R. (1986). Effect of drop breakup on fuel sprays. *SAE transactions*, 218–227.
33. Gavhane, R S.; Kate, A M.; Pawar, A.; Safaei, M. R., Soudagar M; Mujtaba Abbas M. E; Shahapurkar K M.: Effect of zinc oxide nano-additives and soybean biodiesel at varying loads and compression ratios on VCR diesel engine characteristics. Symmetry, 12(6), 1042 (2020)
34. Sadeghinezhad, E.; Kazi, S.N.; Sadeghinejad, F.; Badarudin, A.; Mehrali, M.; Sadri, R.; Safaei, M.R.: A comprehensive literature review of bio-fuel performance in internal combustion engine and relevant costs involvement. Renew. Sustain. Energy Rev. **30**, 29–44 (2014)
35. Samir Naje, A,; Yuvarajan, D.; abed Al-Ridah, Z.; Sandeep, H.; Nagarajan, A: Ignition study of neat biodiesel in dual fueled research engine. Fuel, 281, 118673 (2020)
36. Sateesh, K.A.; Yaliwal, V.S.; Soudagar, M.E.M.; Banapurmath, N.R.; Fayaz, H.; Safaei, M.R.; El-Seesy, A.I.: Utilization of biodiesel/Al2O3 nanoparticles for combustion behavior enhancement of a diesel engine operated on dual fuel mode. J. Therm. Anal. Calorim. **147**(10), 5897–5911 (2022)
37. Sener, R.; Yangaz, M.U.; Gul, M.Z.: Effects of injection strategy and combustion chamber modification on a single-cylinder diesel engine. Fuel **266**, 117122 (2020)
38. Sharma, S.; Sharma, D.; Soni, S. L.; & Singh, D.: Experimental investigation on spark-ignition (SI) engine fuelled with acetylene in dual-fuel mode. Int. J. Ambient Energy, 1–7 (2020)
39. Shen, Z.; Wang, X.; Zhao, H.; Lin, Bo.; Shen, Y.; Yang, J.: Numerical investigation of natural gas-diesel dual-fuel engine with different piston geometries and radial clearances. Energy **220**, 119706 (2021)
40. Shi, Y.; Ge, H.W.; Reitz, R.D.: Computational optimization of internal combustion engines. Springer Science & Business Media (2011)
41. Sonachalam, M.; Manieniyan, V.: Optimization of critical angle, distance and flow rate of secondary fuel injection in DI diesel engine using computational fluid dynamics. SN Appl. Sci. **3**(1), 1–13 (2021)
42. Sonachalam, M.; PaulPandian, P.; Manieniyan, V.: Emission reduction in diesel engine with acetylene gas and biodiesel using inlet manifold injection. Clean Technol. Environ. Policy **22**(10), 2177–2191 (2020)
43. Soudagar, M. E. M.; Afzal, A.; Safaei, M. R.; Manokar, A. M.; EL-Seesy, A. I.; Mujtaba, M. A.; Goodarzi, M: Investigation on the effect of cottonseed oil blended with different percentages of octanol and suspended MWCNT nanoparticles on diesel engine characteristics. J. Therm. Anal. Calorimetry, 1–18 (2020)
44. Soudagar, M.E.M.; Khan, H.M.; Khan, T.M.; Razzaq, L.; Asif, T.; Mujtaba, M.A.; Safaei, M.R.: Experimental analysis of engine performance and exhaust pollutant on a single-cylinder diesel engine operated using moringa oleifera biodiesel. Appl. Sci. **11**(15), 7071 (2021)
45. Soudagar, M.E.M.; Mujtaba, M.A.; Safaei, M.R.; Afzal, A.; Ahmed, W.; Banapurmath, N.R.; Taqui, S.N.: Effect of Sr@ ZnO nanoparticles and Ricinus communis biodiesel-diesel fuel blends on modified CRDI diesel engine characteristics. Energy **215**, 119094 (2021)
46. Sukumar, V.; Manieniyan, V.; Sivaprakasam, S.: Experimental studies on DI diesel engine fueled in sweet lime pyrolysis oil with biodiesel. Int. J. Appl. Eng. Res. **14**(5), 1145–1150 (2019)
47. Sukumar, V.; Manieniyan, V.; Senthilkumar, R.; Sivaprakasam, S.: Production of bio oil from sweet lime empty fruit bunch by pyrolysis. Renew. Energy **146**, 309–315 (2020)
48. Uyumaz, A.: Experimental evaluation of linseed oil biodiesel/diesel fuel blends on combustion, performance and emission characteristics in a DI diesel engine. Fuel **267**, 117150 (2020)
49. Wategave, S.P.; Banapurmath, N.R.; Sawant, M.S.; Soudagar, M.E.M.; Mujtaba, M.A.; Afzal, A.; Sajjan, A.M.: Clean combustion and emissions strategy using reactivity controlled compression ignition (RCCI) mode engine powered with CNG-Karanja biodiesel. J. Taiwan Inst. Chem. Eng. **124**, 116–131 (2021)
50. Wise, D. M.; Olsen, D. B.; Kim, M: Development of a lean burn methane number measurement technique for alternative gaseous fuel evaluation. In *Internal Combustion Engine Division Fall Technical Conference* (Vol. 56109, p. V002T02A014). American Society of Mechanical Engineers (2013)
51. Wulff, J. W.; Hulett, M.; Lee, S.: (2000).U.S. Patent No. 6,076,487. Washington, DC: U.S. Patent and Trademark Office
52. Zhang, Y.; Jia, M.; Liu, H.; Xie, M.; Wang, T.; Zhou, L.: (2014). Development of a new spray/wall interaction model for diesel spray under PCCI-engine relevant conditions. Atomization Sprays, *24*(1)